Design and Synthesis of Molecular Donors for Solution-Processed High-Efficiency Organic Solar Cells

ARTICLE *in* ACCOUNTS OF CHEMICAL RESEARCH · AUGUST 2013

Impact Factor: 22.32 · DOI: 10.1021/ar400136b · Source: PubMed

4 AUTHORS, INCLUDING:

Jessica E Coughlin
University of California, Santa Barbara
8 PUBLICATIONS **226** CITATIONS

ACCOUNTS
of chemical research

Design and Synthesis of Molecular Donors for Solution-Processed High-Efficiency Organic Solar Cells

JESSICA E. COUGHLIN,[†] ZACHARY B. HENSON,[†] GREGORY C. WELCH,[‡] AND GUILLERMO C. BAZAN*,[†]

[†]*Center for Polymers and Organic Solids, Department of Chemistry and Biochemistry, University of California Santa Barbara, Santa Barbara, California 93117, United States, and* [‡]*Department of Chemistry, Dalhousie University, Halifax, Nova Scotia B3H 4R2, Canada*

RECEIVED ON MAY 15, 2013

CONSPECTUS

Organic semiconductors incorporated into solar cells using a bulk heterojunction (BHJ) construction show promise as a cleaner answer to increasing energy needs throughout the world. Organic solar cells based on the BHJ architecture have steadily increased in their device performance over the past two decades, with power conversion efficiencies reaching 10%. Much of this success has come with conjugated polymer/fullerene combinations, where optimized polymer design strategies, synthetic protocols, device fabrication procedures, and characterization methods have provided significant advancements in the technology. More recently, chemists have been paying particular attention to well-defined molecular donor systems due to their ease of functionalization, amenability to standard organic purification and characterization methods, and reduced batch-to-batch variability compared to polymer counterparts.

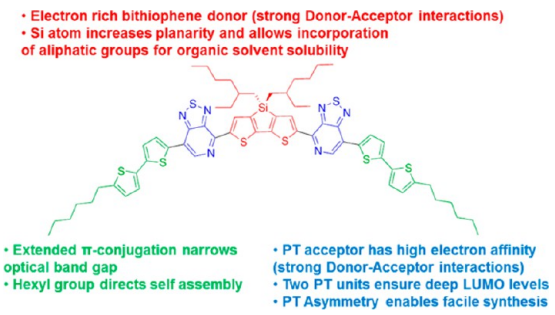

There are several critical properties for efficient small molecule donors. First, broad optical absorption needs to extend towards the near-IR region to achieve spectral overlap with the solar spectrum. Second, the low lying highest occupied molecular orbital (HOMO) energy levels need to be between −5.2 and −5.5 eV to ensure acceptable device open circuit voltages. Third, the structures need to be relatively planar to ensure close intermolecular contacts and high charge carrier mobilities. And last, the small molecule donors need to be sufficiently soluble in organic solvents (≥10 mg/mL) to facilitate solution deposition of thin films of appropriate uniformity and thickness. Ideally, these molecules should be constructed from cost-effective, sustainable building blocks using established, high yielding reactions in as few steps as possible. The structures should also be easy to functionalize to maximize tunability for desired properties.

In this Account, we present a chronological description of our thought process and design strategies used in the development of highly efficient molecular donors that achieve power conversion efficiencies greater than 7%. The molecules are based on a modular D^1-A-D^2-A-D^1 architecture, where A is an asymmetric electron deficient heterocycle, which allowed us to quickly access a library of compounds and develop structure−property−performance relationships. Modifications to the D1 and D2 units enable spectral coverage throughout the entire visible region and control of HOMO energy levels, while adjustments to the pendant alkyl substituents dictate molecular solubility, thermal transition temperatures, and solid-state organizational tendencies. Additionally, we discuss regiochemical considerations that highlight how individual atom placements can significantly influence molecular and subsequently device characteristics.

Our results demonstrate the utility of this architecture for generating promising materials to be integrated into organic photovoltaic devices, call attention to areas for improvement, and provide guiding principles to sustain the steady increases necessary to move this technology forward.

1. Introduction

Organic semiconductors are commonly incorporated into solar cells using a bulk heterojunction (BHJ) construction.[1] The BHJ consists of two components, a p-type (donor) and an n-type (acceptor) semiconductor, which can be deposited simultaneously from solution to form interpenetrating

Published on the Web 08/28/2013 www.pubs.acs.org/accounts
10.1021/ar400136b

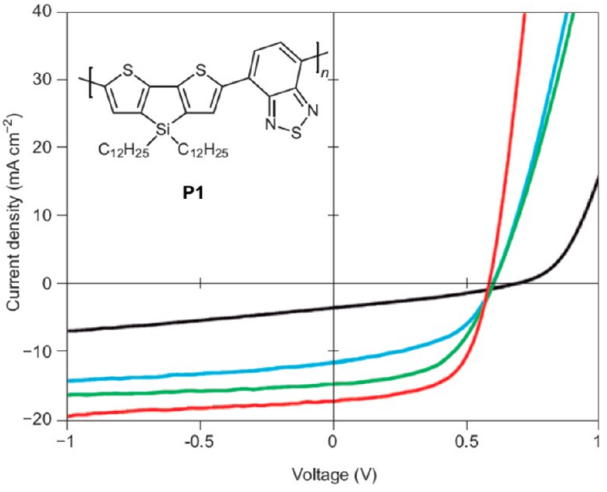

FIGURE 1. Current density–voltage characteristics of **P1** as a function of M_n; black, M_n= 7 kg/mol; blue, 14 kg/mol; green, 25 kg/mol; red, 34 kg/mol.[15] Reproduced with permission from ref 15. Copyright 2009 Nature Publishing Group.

networks that facilitate transport of charge carriers to their respective electrodes. Most commonly used n-type components are fullerene derivatives, such as $PC_{61}BM$ ([6,6]-phenyl-C_{61}-butyric acid methyl ester) and $PC_{71}BM$, due to their solubility in organic solvents, reversible electrochemical reductions, and low lying energy levels.[2] The latter set the stage for the thermodynamically favorable photoinduced electron transfer from the donor counterparts. Donor materials have undergone significant diversification over time and includes polymer systems[2−4] and discrete molecules.[5] Because of the limited absorption by fullerenes, the majority of sunlight-induced photoexcitations (excitons) occur in the donor material. These excitons diffuse until they reach a donor/acceptor interface, where electron transfer to the acceptor takes place.[6] Electrons migrate through the acceptor and holes through the donor phase to the respective electrodes. Although mechanistic understanding of organic photovoltaic device (OPVs) operation remains under debate,[7] there is sufficient information for rational molecular design. However, there are important general limitations on our ability to translate molecular design to bulk performance and some of these arise from the specific organizational requirements of the BHJ layer. For example, it is not clear to what degree the molecular connectivity may favor the most desirable BHJ configuration. Order within the donor or acceptor phases is also important for maximizing charge carrier mobilities. Optimal solar cell operation therefore requires control over molecular properties, as well as the forces that lead to the desired organization during kinetically constrained film formation, and/or via post deposition treatments.[8]

A substantial body of literature exists on narrow band gap conjugated polymers,[3,4,9−12] though molecular donors have begun to attract a greater share of the attention.[13] Part of this shift is a result of batch-to-batch variability in polymer-based devices, reasonably attributed to variations in molecular weight, polydispersity, and impurity levels. In contrast, molecular systems are monodisperse and can be purified using common organic chemistry techniques. Our group recently reported a series of high performance molecular donors and has begun to elucidate structure–property–performance relationships. This Account provides a largely chronological perspective of the efforts and design criteria that led us to these molecular systems. It extracts from a series of papers certain chemistry-centric principles we have found to be successful at this point of our studies.

2. The Influence of Molecular Weight Characteristics on Solar Cell Performance

Interest in the aggregation tendencies of narrow band gap conjugated polymers with solvent additives and how they impact power conversion efficiencies (PCEs) led us to examine the effect of molecular weight on device characteristics.[14] Focusing on a dithienosilole-*alt*-benzothiadiazole based copolymer, a systematic screening of the polymerization process, including varying monomer ratios and reaction conditions, was performed. Reasonably high molecular weight samples could be synthesized reproducibly; reaction times were also reduced from the several days required by conventional heating to a few hours by microwave irradiation.[15] The molecular weight of polymer samples was found to influence device performance. As shown in Figure 1 for P1, the PCE increases from 1.2% to 5.9%, with increasing number average molecular weight (M_n) from 7 to 34 kg mol^{-1}.[15,16] A similar dependence has been observed in the case of poly(3-hexylthiophene) (P3HT).[17] Changes in PCE as a function of subtle polymer characteristics make it difficult to address how variations in molecular structure can lead to enhancements in device function. These frustrations played an important role in our interest in designing molecular donor systems.

3. Lewis Acid Adducts of Narrow Band Gap Chromophores

Concomitant with our progress preparing high M_n polymers, our group was examining the influence of Lewis acids on the optical properties of conjugated systems.[18,19] Figure 2 illustrates a simplified perspective of the anticipated impact on the absorption of a donor/acceptor chromophore.

Upon linking and hybridization of the molecular orbitals of D and A_1, one can expect an optical transition much narrower than if two identical aromatic fragments are conjugated with each other (Figure 2 left).[20] Although often neglected from consideration in materials design, available electron lone pairs are noteworthy, particularly in that they can interact with Lewis acids. If, for example, the Lewis acid $B(C_6F_5)_3$ binds to a nitrogen lone pair in BT, withdrawal of electron density from the π-conjugated framework shifts the HOMO and LUMO of the acceptor moiety (now A_2) to lower energies. The electron affinity of the acceptor moiety is thus increased (D-A^2, Figure 2 right). Hybridization of this adduct with DTS would reasonably result in a narrowing of the gap, when compared to the chromophore bearing unmodified BT.

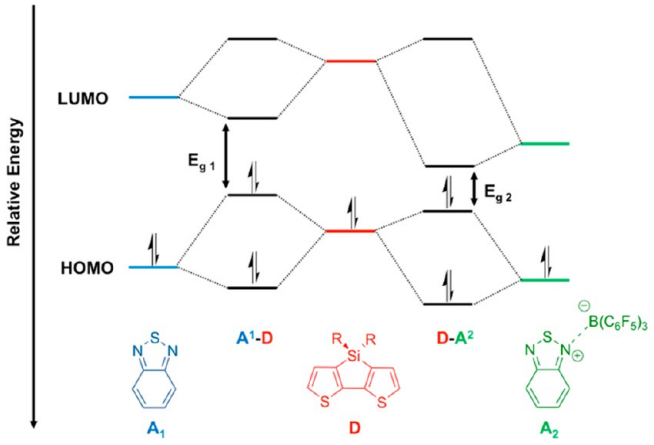

FIGURE 2. Schematic representation of how binding a Lewis acid to an acceptor fragment leads to a narrowing of the optical gap. Binding the Lewis acid results in a synergistic lowering of both the HOMO and LUMO energy levels with the LUMO being the most affected, thus narrowing the band gap.

In the case of 5,5′-bis(benzo[2,1,3]thiadiazole)-3,3′-di-*n*-dodecylsilylene-2,2′-bithiophene (**1**), shown in Figure 3, one observes a change in the absorption maximum (λ_{max}) from ~500 to ~650 nm upon $B(C_6F_5)_3$ coordination to the nitrogen atoms in the BT units. Addition of Lewis bases stronger than BT, such as triphenylphosphine, results in regeneration of the original absorption. Moreover, the absorption properties can

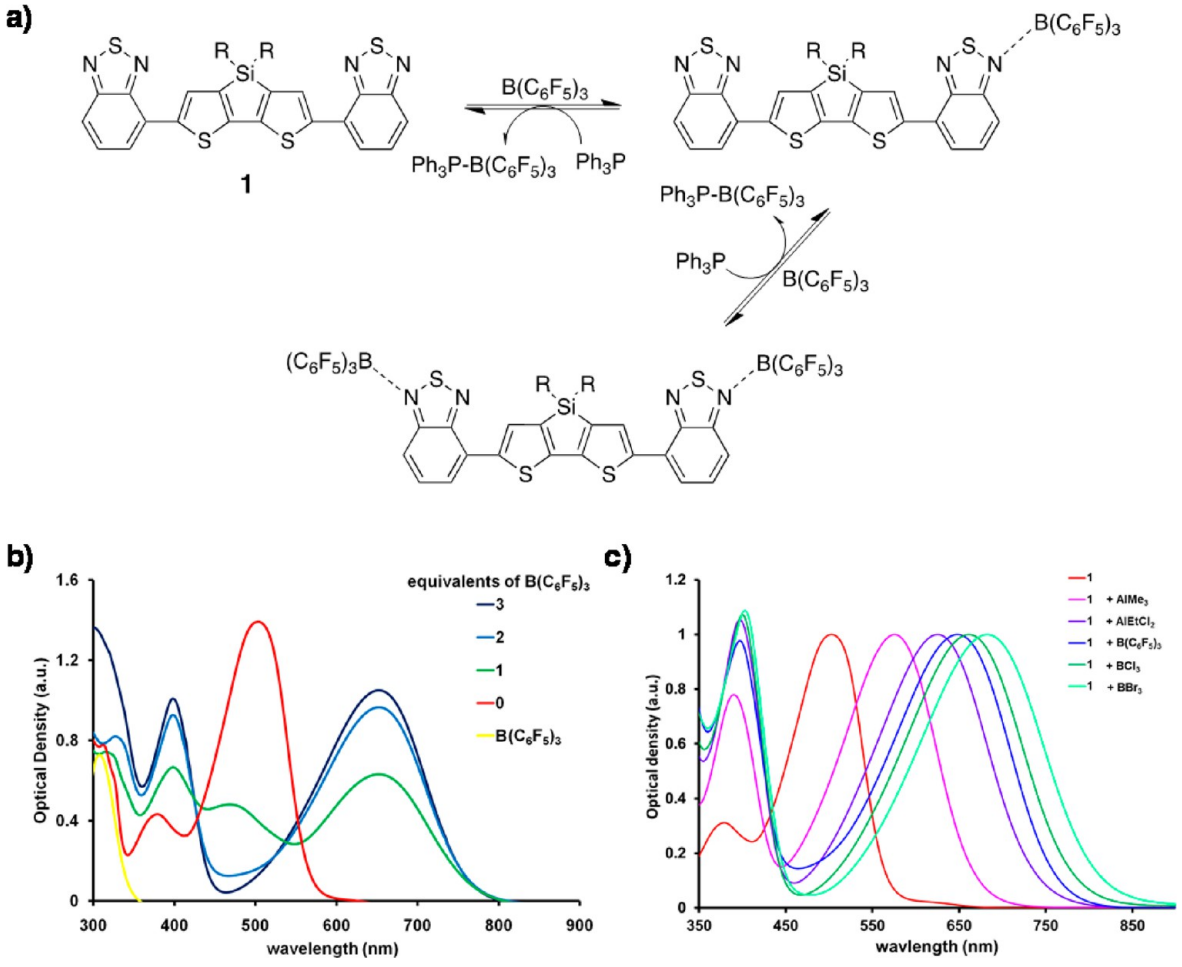

FIGURE 3. (a) Addition of $B(C_6F_5)_3$ to **1**. (b) Absorption spectra of **1** upon the addition of different equivalents of $B(C_6F_5)_3$. (c) Absorption spectra of **1** upon addition of different Lewis acids. Reproduced with permission from ref 18. Copyright 2009 American Chemical Society.

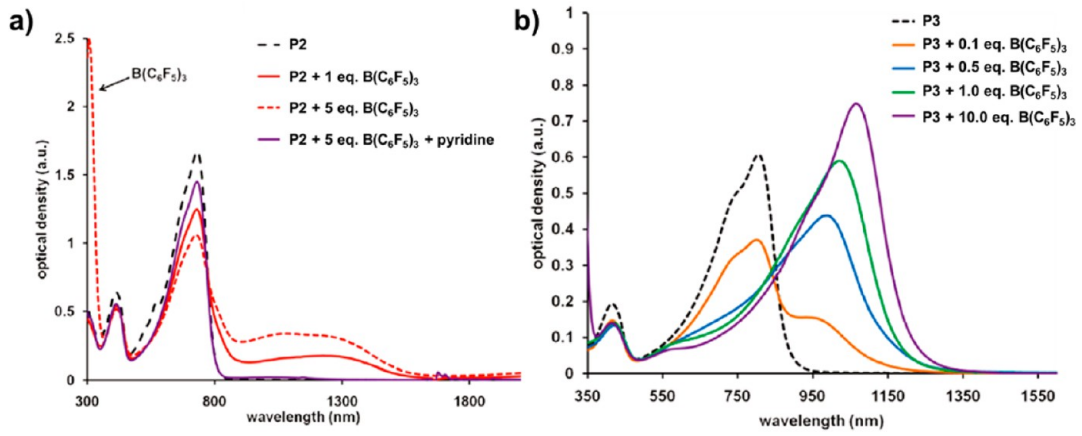

FIGURE 4. Absorption spectra of (a) **P2** and (b) **P3** upon addition of $B(C_6F_5)_3$ in solution. Reproduced with permission from ref 19. Copyright 2011 American Chemical Society.

SCHEME 1[a]

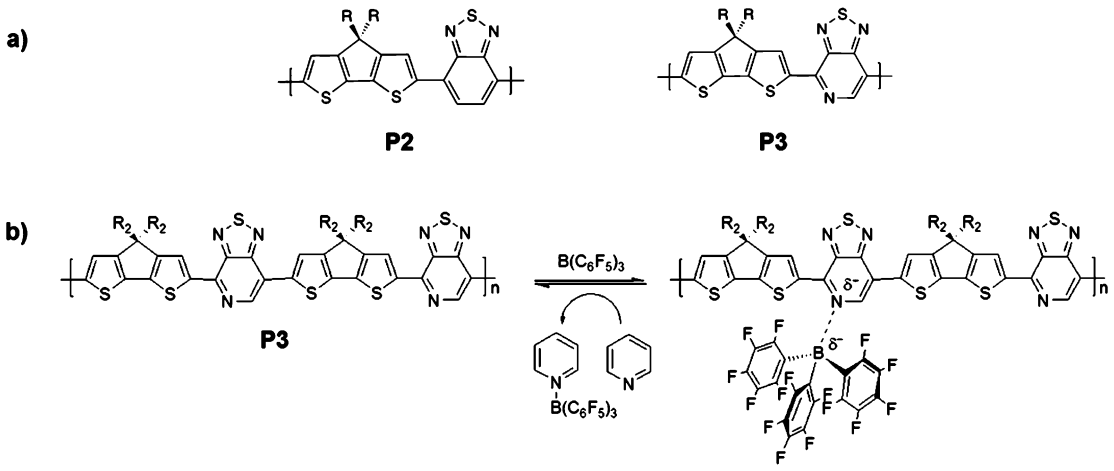

[a](a) Structures of **P2** and **P3**. (b) Addition of $B(C_6F_5)_3$ to **P3**. R, R_2 = alkyl.

be tuned by varying the strength of the Lewis acid, with the strongest Lewis acid providing the greatest red shift (Figure 3c).[18]

We attempted to extend this strategy to polymer systems, such as **P2** in Scheme 1, but could not reach similar binding as for **1** (Figure 4a). Model compounds revealed that steric constraints about the azole nitrogen in polymer architectures inhibited adduct formation.[19] Based on the known affinity of $B(C_6F_5)_3$ to bind pyridine, we turned our attention to [1,2,5]thiadiazolo[3,4-c]pyridine (PT) as a replacement for BT. PT is a strong electron acceptor, which can lead to charge-transfer characteristics when coupled with complementary donor fragments, and also offers a pyridyl nitrogen atom that is more basic and accessible than the azole counterpart in BT. Indeed, adduct formation became possible for conjugated polymer systems containing the PT fragment. Specifically, **P3** in Scheme 1 was synthesized and exhibited much greater propensity to bind $B(C_6F_5)_3$, compared to **P2** (Figure 4b) . The utility of using Lewis acids to tune the optical band gap of polymer materials via coordination to pyridyl N-atoms has recently been extended to wide-band gap materials for use in organic light emitting diodes.[21]

4. PT-Based Chromophores

Electrochemical studies and theoretical modeling of the Lewis acid−chromophore interaction showed that the PT-based chromophores had HOMO and LUMO energy levels that could be tuned near the vicinity of values desirable for integration into OPV layers.[22−24] Furthermore, a key advantage in synthetic simplicity can be realized with PT due to its asymmetry. Similar to 2,5-dibromopyridine,[25] one finds with 4,7-dibromo-[1,2,5]thiadiazolo[3,4-c]pyridine ($PTBr_2$) that the bromine adjacent to the pyridyl nitrogen is more reactive

SCHEME 2[a]

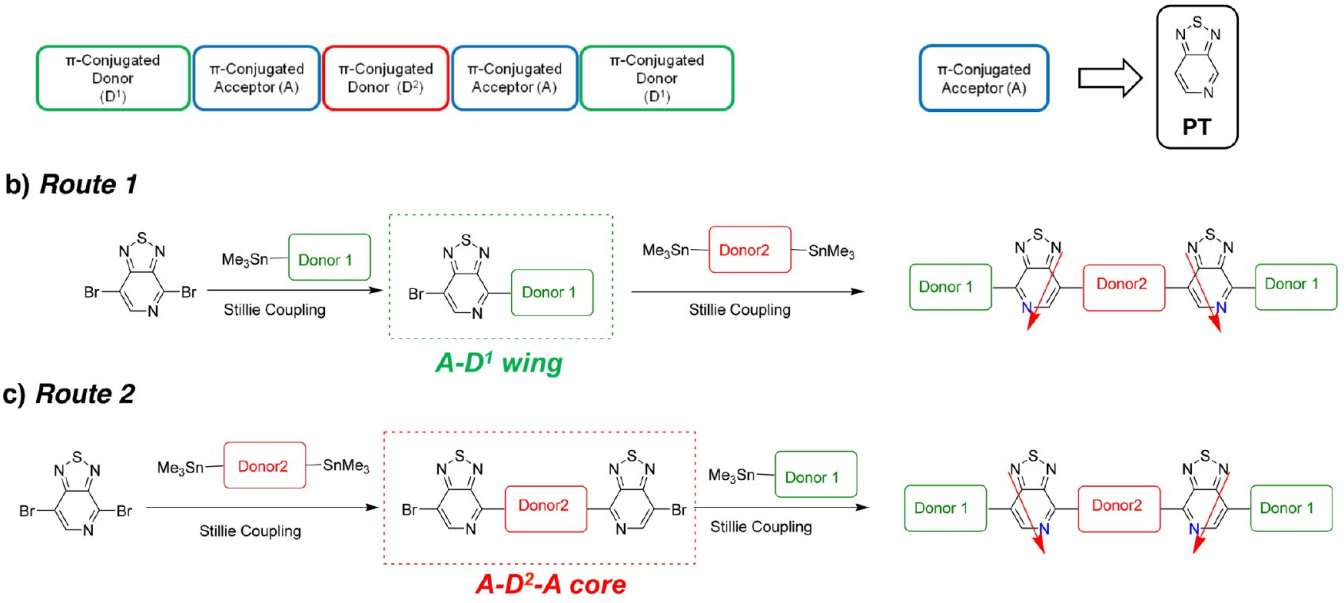

[a](a) General structure of chromophores with a D^1-A-D^2-A-D^1 architecture. Synthetic entry into D^1-PT-D^2-PT-D^1 molecules with (b) distal regiochemistry and (c) proximal regiochemistry.

toward stannylated aromatic compounds.[26] Scheme 2 shows how site-selective Stille coupling can be used to quickly generate molecules that can be generally described by a D^1-A-D^2-A-D^1 conjugated framework. D and A correspond to the electron rich and poor aromatic moieties, respectively, that lead to charge transfer excited states and absorption profiles useful for sunlight harvesting. Within this architecture, PT corresponds to "A". For example, reaction of 1 equiv of R_3Sn-D^1 (R = methyl, butyl) with $PTBr_2$ provides monosubstituted BrPT-D^1 in which the pyridyl nitrogen points toward D^1. Reaction of BrPT-D^1 with R_3Sn-D^2-SnR_3 completes the synthesis, yielding the D^1-PT-D^2-PT-D^1 framework in which the pyridyl N atoms are in a *distal* regiochemistry; that is, both are located away from D^2 (Scheme 2b). If one starts the synthetic sequence by the reaction of R_3Sn-D^2-SnR_3 with $PTBr_2$, followed by workup and addition of R_3Sn-D^1, then the D^1-PT-D^2-PT-D^1 product has the two pyridyl nitrogen atoms in a *proximal* orientation; that is, both are adjacent to the center of the chromophore (Scheme 2c).

5. Selection Criteria

By virtue of the modular synthetic route in Scheme 2, it is possible to access a wide range of D^1-PT-D^2-PT-D^1 molecules. It became evident that the capacity to generate ever-larger libraries of compounds would overwhelm capabilities available for sorting through the matrix of device optimization variables specific for each new material. A new challenge then arises: given the trial and error nature of device optimization, how does one "bet" on molecular systems that have the best chance of yielding high performance solar cells? Empirical criteria were thus set up to rank order the probability of success in device configurations. We provide our perspective of this process by examination of compounds **2**–**14** in Figure 5 within the context of four critical features: (i) broad optical absorption, (ii) low lying HOMO energy levels, (iii) planar structures with good intermolecular contacts, and (iv) solubility in excess of 10 mg/mL.

(i). Broad, Extended Optical Absorption. One requirement for obtaining photovoltaic devices with high PCE values is the ability to effectively harness the solar spectrum. Molecules with broad absorption features extending throughout the visible and into the near-IR region of the spectrum are appealing, and may lead to devices with high short circuit current values (J_{sc}). In this section, we discuss modifications to the D^1-A-D^2-A-D^1 architecture capable of influencing the absorption features.

First, we investigated the role of conjugation length of the D^1. Three compounds with end group donors (D^1) containing one (**2**), two (**3**), and three thiophenes (**4**) were examined, and revealed that the optical band gap decreased as a function of increasing conjugation length (Figure 6a,b). This reduction was greater when increasing from one thiophene to two (1.63–1.51 eV), than when increasing from two to three thiophenes (minimal change in optical band gap). Thus one concludes that D^1 with two aromatic rings is sufficient to maximize optical absorption within this architecture.

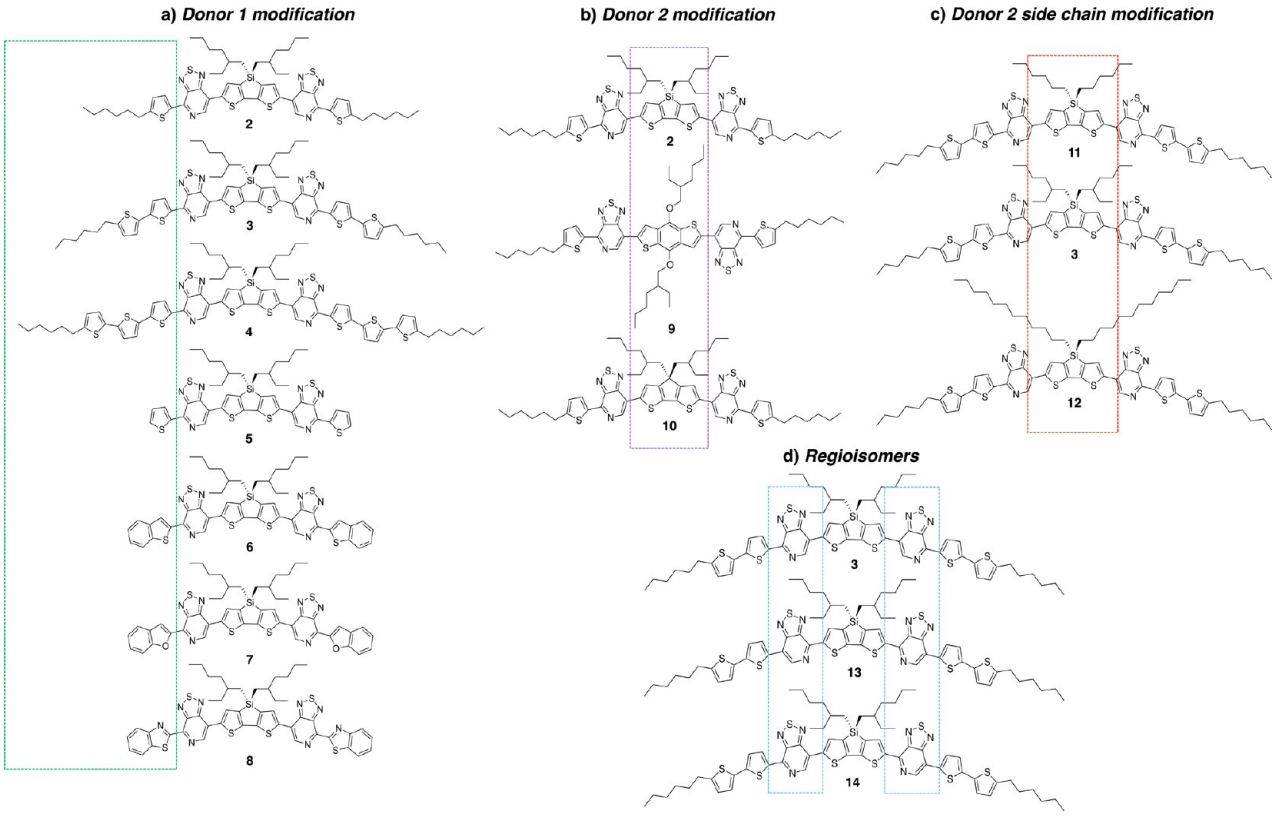

FIGURE 5. Molecular structures of compounds **2**–**14**, grouped in sets that focus on related structural variations.

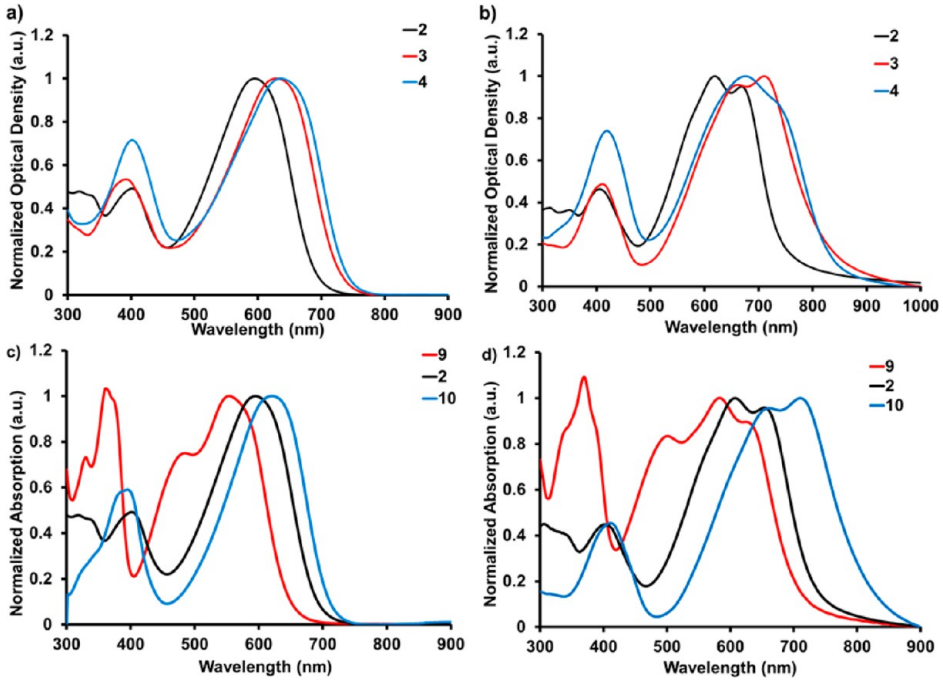

FIGURE 6. Solution absorption spectra of (a) **2**, **3**, and **4** and (c) **9**, **2**, and **10** in $CHCl_3$. Thin film absorption spectra of (b) **2**, **3**, and **4** and (d) **9**, **2**, and **10** on quartz. Reproduced with permission from ref 27. Copyright 2012 American Chemical Society.

We next considered three D^2 alternatives, while keeping the PT-D^1 module constant, including DTS (**2**), benzodithiophene (BDT) (**9**), and CDT (**10**) (Figure 5b). In solution, one observes for **9** a more blue-shifted and more

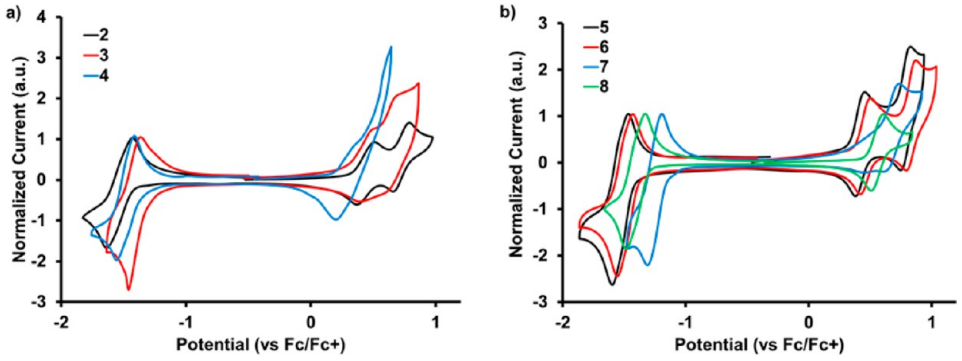

FIGURE 7. CV of (a) **2**, **3**, and **4** and (b) **5**, **6**, **7**, and **8** in CH_2Cl_2. Reproduced with permission from ref 27. Copyright 2012 American Chemical Society.

vibronically defined absorption profile (Figure 6c), relative to **2** and **10**, consistent with its less electron rich and more rigid structure. Compounds **2** and **10** exhibit small differences in absorption onset in solution, but significant differences as thin films (Figure 6d). While the enhanced absorption of **10** relative to **2** is attractive, the DTS core was deemed a better choice than CDT as a central donor core due to its ability to lead to more ordered arrangements in the solid state, as evidenced from solid state absorption and differential scanning calorimetry (DSC) and in agreement with observations from polymer systems.[27]

(ii). Low Lying HOMO (−5.2 to −5.5 eV). As discussed above, molecules with extended absorption allow collection of the maximum amount of photons and therefore have potential for high J_{sc} devices. Therefore, narrowing the optical band gap is an important strategy to achieve high PCE devices. However, because of the empirical relationship between the open circuit voltage (V_{oc}) and the HOMO energy of the donor molecule, overextending the absorption may lead to poorly performing devices if the narrowing of the gap results from an increase in the HOMO energy level. A balance must be found to provide materials with suitable absorption properties and deep enough HOMO energy levels capable of producing high V_{oc}.

Extension of the conjugation length through the D^1 as a function of the number of thiophenes provided an increase in the HOMO energy as shown by the cyclic voltammetry in Figure 7a (see also Table 1). This is likely due to the larger number of electron rich rings and is generally undesirable. To lower the HOMO levels, different D^2 units of increasing electron affinity were also investigated. Using thiophene (**5**), benzothiophene (**6**), benzofuran (**7**), and benzothiazole (**8**) end-caps (Figure 5a) allowed for a systematic lowering of the energy levels from **5** to **8**, consistent with benzothiazole having the highest electron affinity. Unfortunately, the lack of aliphatic substituents within these D^1 blocks results in **5**−**8** having poor solubilities and presented challenges for exploiting their desirable attributes in device configurations.

TABLE 1. HOMO and LUMO Energy Levels Determined by Cyclic Voltammetry

	cyclic voltammetry[a]	
compd	HOMO (eV)	LUMO (eV)
2	−5.20	−3.48
3	−5.16	−3.61
4	−5.07	−3.55
5	−5.20	−3.47
6	−5.26	−3.55
7	−5.34	−3.60
8	−5.42	−3.75

[a] HOMO $= -e(4.88\ \text{V} + E_{ox}^{Fc/Fc+})$, where $E_{ox}^{Fc/Fc+}$ = oxidation onset vs ferrocene. LUMO $= -e(4.88\ \text{V} + E_{red}^{Fc/Fc+})$, where $E_{red}^{Fc/Fc+}$ = reduction onset vs ferrocene.

(iii). Thermal Stability and Ordered Structures. Aliphatic side chains not only affect material solubility, but also impact self-assembly. Obtaining materials capable of self-assembling into ordered domains with close intermolecular contacts is desirable for achieving favorable charge transport. We found that varying the alkyl chain D^2 unit of the molecule led to modifications in both material solubility and thermal properties without significantly influencing the absorption properties (Figure 8a). Increasing the chain length from hexyl (**11**) to ethyl hexyl (**3**) to dodecyl (**12**) (see Figure 5c) brought a lowering of both the melting and crystallization transition temperatures observed by DSC (Figure 8b,c) and an increase in solubility (vide infra). This can be attributed to tighter packing in the solid state for the shorter alkyl chain molecule.

Individual atom placements can also influence organizational tendencies, as seen when comparing the three regioisomers **3**, **13**, and **14** (Figure 5d), in which the position of the PT pyridal nitrogens are in different arrangements. Thin film absorption of the three regioisomers reveals variations in the proportion of the two peaks between 500 and 800 nm (Figure 8d). This lower energy feature is often attributed to enhanced orbital overlap due to a more aggregated state and may suggest a less ordered thin film in the case of the

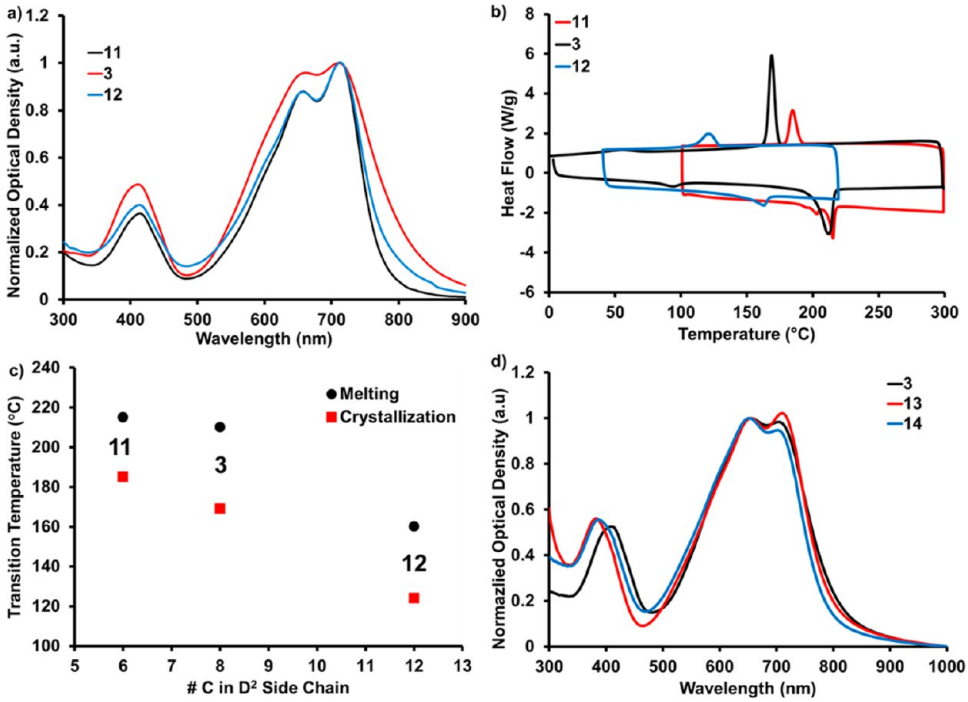

FIGURE 8. (a) Thin film absorption spectra of **11**, **3**, and **12** on quartz. (b) DSC traces of **11**, **3**, and **12**. (c) Melting and crystallization transition temperature as a function of carbons on the D^2 side chain. (d) Thin film absorption of regioisomers **3**, **13**, and **14**. Reproduced with permission from ref 27. Copyright 2012 American Chemical Society.

asymmetric molecule (**14**). A more detailed discussion of the influences of single atom substitutions comes in section 7.

(iv). Solubility Exceeding 10 mg/mL. Solubility is necessary when considering molecules for device fabrication using high throughput methods. Because small molecules form less viscous solutions than polymers, we targeted solubilities above 10 mg/mL for device integration. A few comments on the solubility trends follow. Not surprisingly, as the conjugation length increases (i.e., the ratio of aromatic units to solubilizing side chains), one observes a decrease in solubility. For example, **2** has solubility in chloroform in excess of 50 mg/mL, while **4**, which contains four additional thiophenes, has solubility below 10 mg/mL (Figure 9a). The solubility can also be influenced by the length and topology of the solubilizing alkyl chains. Figure 9b shows that the solubility increases as the number of carbons in the alkyl chain increases from six (**11**) to eight (**3**) to twelve (**13**) carbons. Interestingly, **3**, which contains a branched alkyl chain has solubility close to that of **13** even though it has four fewer carbon atoms in the side chain, reflecting the ability of branched alkyl chains to effectively solubilize these chromophores. It is also worth noting that compounds **6**-**8** with unsubstituted D^1 end groups have solubilities less than 10 mg/mL, and were not considered viable candidates.

6. Importance of Fabrication Conditions and Donor Purity

From the collected set of observations above, we focused device fabrication efforts using **3** and **13**. First we explored the ITO/HTL/**3**:$PC_{71}BM$/Al device architecture, where ITO is indium tin oxide and the hole transport layer (HTL) is a doped polythiophene used to manage charge extraction.[26] Through variations in **3**/$PC_{71}BM$ ratios and thermal annealing temperatures, it was possible to reach a PCE value of ~3%. Two device fabrication modifications proved critical for achieving a major breakthrough: (1) the use of a molybdenum oxide (MoO_x) HTL and (2) the use of diiodooctane (DIO) as a solvent additive. Interestingly, for ITO/MoO_x/**13**:$PC_{71}BM$/Al devices, one finds a steep dependence of PCE with respect to [DIO], with the optimized values occurring in a different concentration regime than for polymer systems (1−5%).[28,29] Excellent performance (PCE = 6.7%) is found when 0.25% v/v DIO is added to chlorobenzene, but the device fails nearly completely with 1% v/v DIO.[30] Also worth noting is that typical polymer systems that perform well use an excess of fullerene. For most of the molecular donor systems we have studied, the ratio is reversed, for example, the optimal **13**/$PC_{71}BM$ ratio is 70:30 (Figure 10b).[27,30−33]

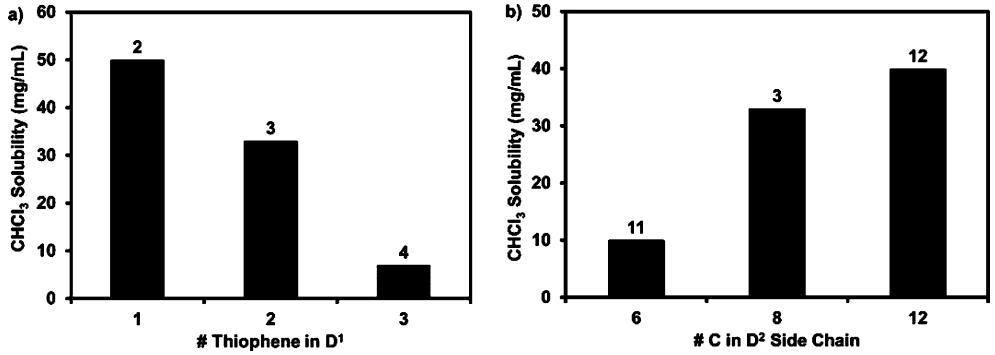

FIGURE 9. Chloroform solubility as a function of (a) number of thiophene heterocycles in D^1 and (b) length of solubilizing alkyl chain on D^2.

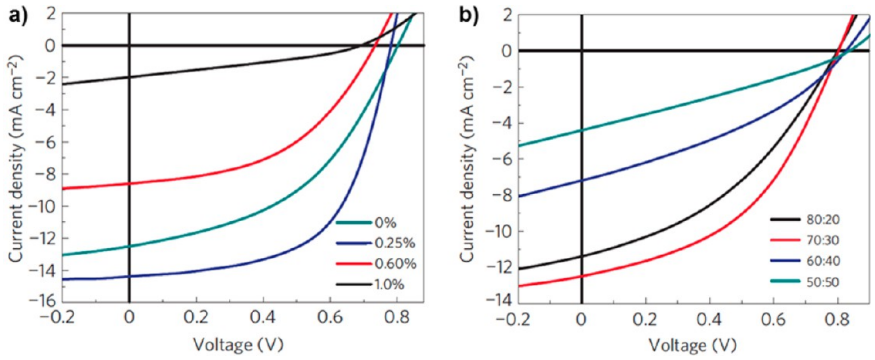

FIGURE 10. (a) Current−voltage (*J*−*V*) characteristics of solar cell devices based on **13**:$PC_{71}BM$ with respect to wt % DIO. b) *J*−*V* characteristics of solar cell devices based on **13**:$PC_{71}BM$ with different blend ratios. Reproduced with permission from ref 30. Copyright 2011 Nature Publishing Group.

Analytically pure materials are critical for achieving reproducible device performance. When using a scaled up batch of **13** we encountered challenges in repeating high device performance. Although not obvious from NMR spectroscopy, mass spectrometry allowed us to identify an impurity, which was assigned to species **15** (Figure 11).[34] This species results if methyl transfer occurs instead of hexylbithiophene transfer, a side reaction that becomes more problematic at higher temperatures. While material purity will always remain an important factor in realizing high performance, small molecules offer an advantage over polymers since trace organic contaminants can be identified and removed.

7. Impact of Regioisomers and Single Atom Substitutions

Figure 12 compares the GIWAXS patterns from blends containing **13**, **3**, **14**, and compound **16**, a nearly isostructral analog in which PT has been substituted with BT.[35] One observes a greater tendency for ordering with the PT-containing compounds; a feature that is confirmed by high-resolution transmission electron microscopy measurements, where 15−30 nm crystalline domains are evident for the PT-containing molecules. Of relevance is that the presence of donor crystallites correlates with the performance of devices prepared with similar compositions (donor/$PC_{70}BM$ = 70:30); PCE(%): 6.7(**13**), 5.6(**3**), 3.0(**14**), and 0.2(**16**). There is a proposal for the absence of crystallization with **16**: DFT calculations show greater variation in molecular electrostatic dipoles as a function of rotational isomers in **16** relative to **13**, and a steeper conformational energy surface for **16**. These conditions provide a greater "mix" of conformers in **16** that negatively impacts self-assembly into crystalline lattices.[35]

A comparison of the crystallographically determined connectivity of **7** (D^1 = benzofuran), and its proximal analog **17** (Figure 13a), revealed how regiochemistry impacts molecular shape.[36] These molecules are significantly bent and the bend angle for **17** is smaller relative to **7** (112.0° vs 116.1°). This difference is attributed to the ability of pyridyl nitrogens to interact with sulfur atoms within the D^2 unit, which provides a driving force for molecular deformation.[26,37] Compound **7** is also less soluble in common organic solvents and provides larger crystallites in spin-cast films; considerations that are relevant for active layer deposition. Changes in molecular shape were also identified as a function of isoelectronic bridging atom substitution (C vs

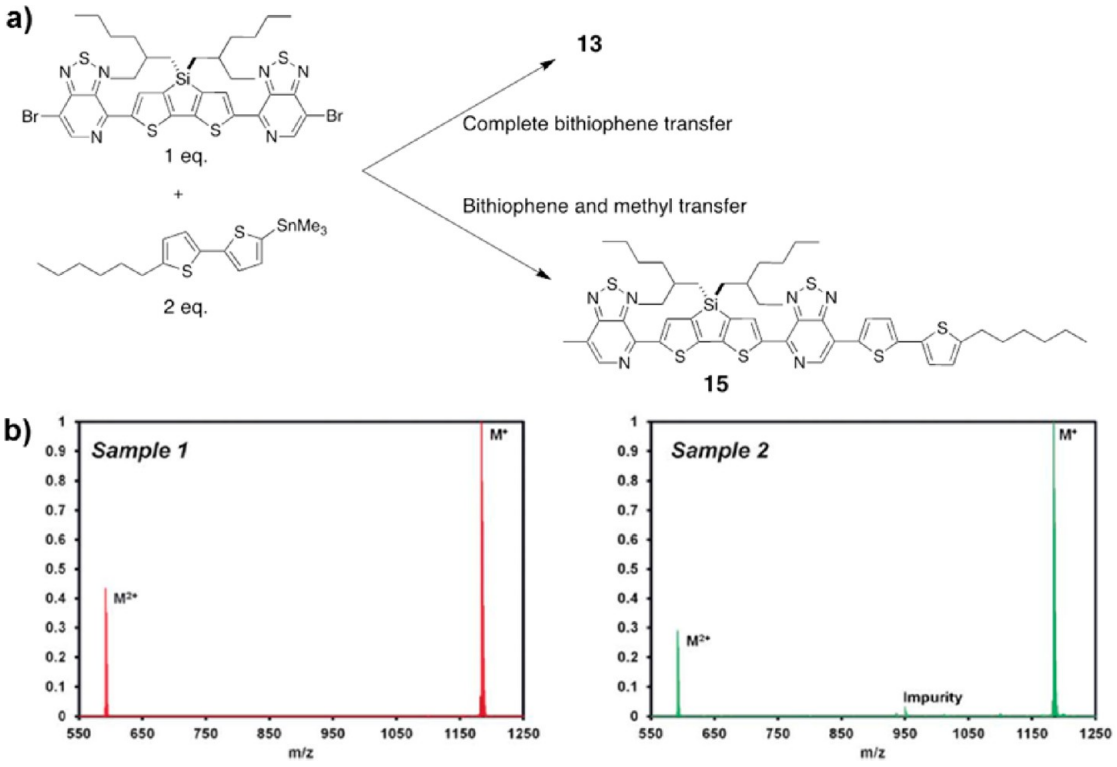

FIGURE 11. (a) Proposal of how impurity **15** arises during Stille cross-coupling. (b) Field desorption mass spectrometry of two samples, with sample 2 showing the presence of **15**. Reproduced with permission by the Royal Society of Chemistry from ref 34.

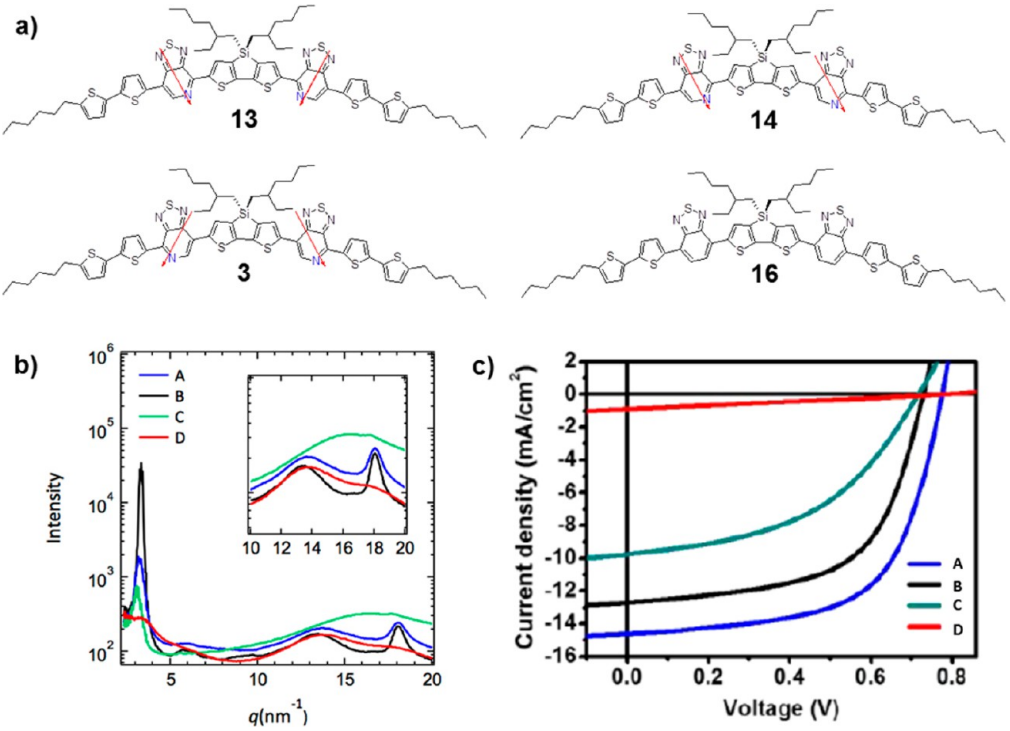

FIGURE 12. (a) Comparison of molecular structures. (b) GIWAXS of blends cast from chlorobenzene and 0.25% DIO containing (A) **13**:$PC_{71}BM$, (B) **3**:$PC_{71}BM$, (C) **14**:$PC_{71}BM$, and (D) **16**:$PC_{71}BM$. (c) $J-V$ curves of 70:30 (w/w) of (A) **13**:$PC_{71}BM$, (B) **3**:$PC_{71}BM$, (C) **14**:$PC_{71}BM$, and (D) **16**:$PC_{71}BM$ cast from chlorobenzene and 0.25% DIO. Reproduced with permission from ref 35. Copyright 2012 American Chemical Society.

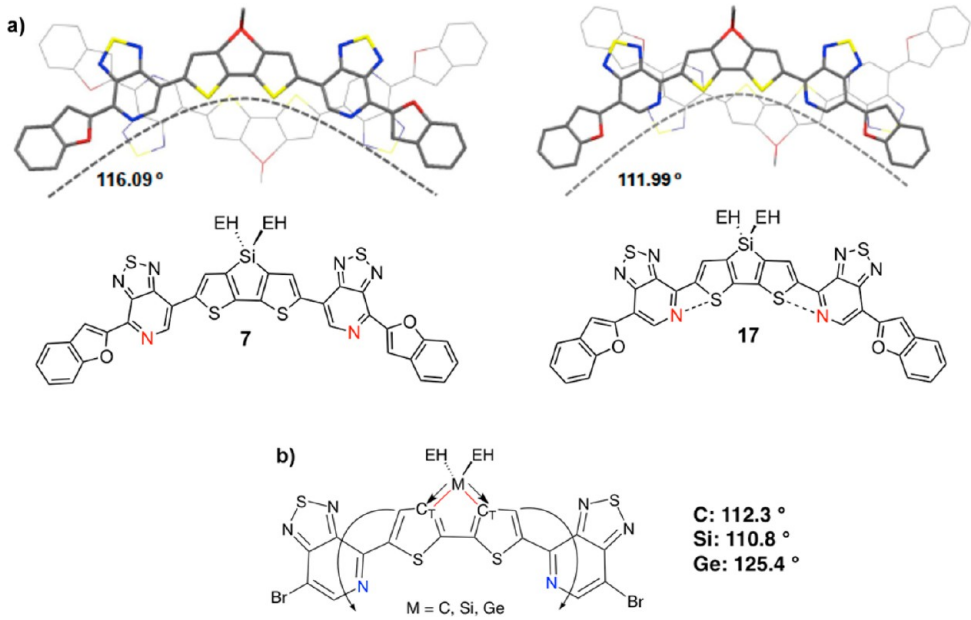

FIGURE 13. (a) Single crystal X-ray analysis of **7** and **17** with a face on view highlighting bend of molecule and intermolecular face-to-face stacking. (b) Molecular bend angle as a function of bridgehead atoms carbon, silicon and germanium. Reproduced with permission from ref 36. Copyright 2013 American Chemical Society.

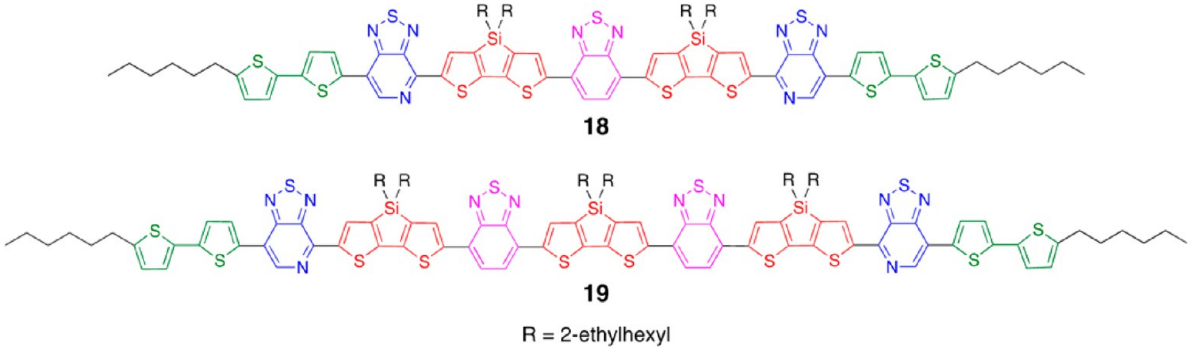

FIGURE 14. Molecular structures of **18** and **19**.

Si vs Ge) in D^2. As the length of the M-C_T bond increases proportionally to the covalent radii of M, (76 pm, C; 111 pm, Si; 120 pm, Ge) there is a commensurate change in the molecular bend (125.4°, C; 112.3°, Si; 110.8°, Ge) (Figure 13b). Thus, it is possible to modify molecular shape, thermal stability and crystallization tendencies via single atom substitutions. However, we lack the ability to completely predict bulk behavior from a simple consideration of molecular connectivity.

8. Larger Sized PT-Containing Chromophores

Molecular size and conjugation length effects were also examined.[33] From a practical perspective, such systems were anticipated to exhibit more thermally robust crystalline phases. The two molecules used for this study, which can be expressed as D^1-A^1-D^2-A^2-D^2-A^1-D^1 (**18**; A^1, blue; A^2, purple) and D^1-A^1-D^2-A^2-D^2-A^2-D^2-A^1-D^1 (**19**), are shown in Figure 14. Since the D and A moieties are similar to the structural units in D−A polymeric analogs, the study of **18**/**19** provides a unique bridge to study how relevant properties change in the continuum between monodisperse molecules and polymers. Figure 16(a) shows a pronounced increase in T_m with molecular size: **13** (209 °C) → **18** (246 °C) → **19** (269 °C). Organic field effect transistors (OFETs) indicate that charge carrier mobilities of **18** and **19** are slightly lower than **13**, but devices maintain function over a wider temperature range, even beyond 200 °C!

Figure 15c shows the current/voltage curves of solar cells containing **18**/$PC_{61}BM$ (60:40, PCE = 5.8%) and **19**/$PC_{61}BM$ (50:50, PCE = 6.5%) blends *directly* cast from chloroform. It is

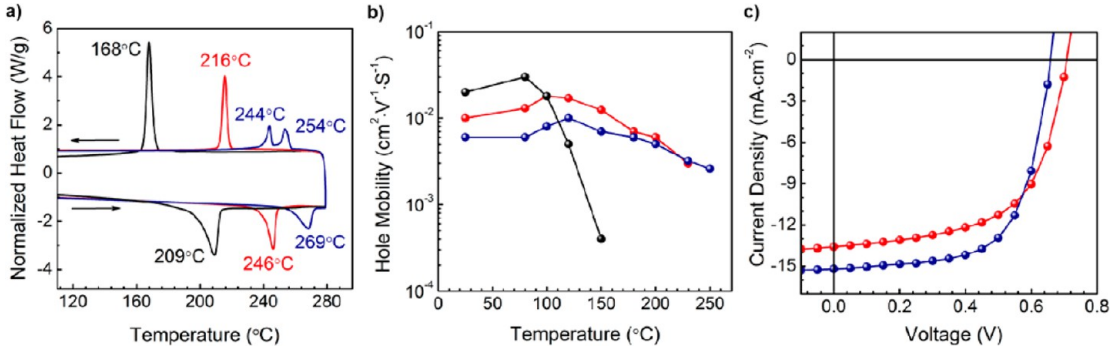

FIGURE 15. Comparison of **13** (black), **18** (red), and **19** (blue): (a) DSC traces. (b) Hole mobility as a function of annealing temperature. (c) *J*–*V* curves of optimized solar cells. Reproduced with permission from ref 32. Copyright 2012 American Chemical Society.

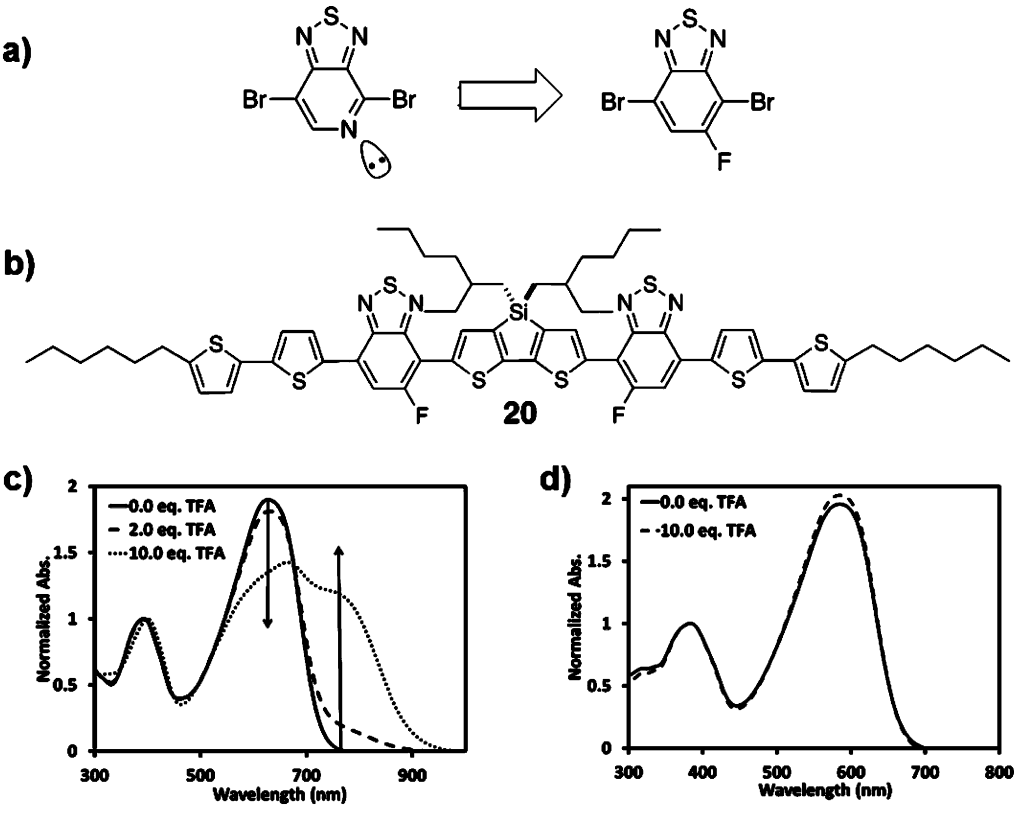

FIGURE 16. (a) Structural evolution from PT to FBT. (b) Molecular structure of compound **20**. (c) UV–visible spectra of compound **13** upon addition of trifluoroacetic acid (TFA). (d) UV–visible spectra of compound **20** upon addition of TFA. Reproduced with permission from ref 33. Copyright 2012 Wiley Wiley-VCH Verlag GmbH & Co. KGaA.

worth recalling that, for **13**, in the absence of solvent additives or thermal annealing, one obtains the best performance (PCE = 4.5%) at a **13**:$PC_{71}BM$ composition ratio of 70:30. D/A loadings of greater than 50% are often observed with molecular systems vs conjugated polymer counterparts. However, with increases in molecular length, one finds a shift in the optimal composition ratio: 60:40 for **18**:$PC_{61}BM$ and 50:50 for **19**:$PC_{61}BM$; conditions that are similar to those broadly required for conjugated polymers. Of further note is that the optimal performance achieved for the **19**:$PC_{61}BM$ combination is relatively insensitive to the composition ratio.

9. Resisting Protonation of PT

We return here to the challenges encountered when fabricating devices atop PEDOT:PSS. Through a collaboration with colleagues at the National Renewable Energy Laboratory (NREL) and the Center for Interface Science: Solar Electric Materials at the University of Arizona, it was determined using XPS and absorption spectroscopy that there is

protonation of the PT fragment by the acidic PSS.[31] This process is reminiscent of the interaction with Lewis acids in Scheme 2 and leads to the formation of interfacial dipoles that interfere with hole-extraction and cause low PCE values. The 5-fluorobenzo[*c*][1,2,5]thiadiazole (FBT) fragment was expected to have a similar electron affinity to PT, but be resistant to acid, and led to the design of **20** in Figure 16.[38,39] Also provided in Figure 16 are the absorption profiles obtained when **13** and **20** are treated with trifluoroacetic (TFA) acid. The absence of a red shift in absorbance observed with **20** indicates negligible sensitivity toward acids. Solar cells were therefore fabricated with the architecture ITO/PEDOT:PSS/**20**:$PC_{71}BM$/Ca/Al, which showed PCE values of 7% (V_{oc} = 809 mV, J_{sc} = 12.8 mA cm^{-2}, and FF = 0.68).[32] A relevant message here is the importance of characterization of interfacial chemistry and how aromatic heterocycles of equivalent electronic and optical properties can be chosen to circumvent molecular level events that impact the overall solar cell function.

10. Outlook

Even though it is possible to obtain internal power conversion efficiencies approaching 100% with the ITO/PEDOT:PSS/**20**:$PC_{71}BM$/Ca/Al devices, the molecular design for solar cell fabrication is not finished. There is no obvious basis for understanding how the kinetics of film formation impacts the BHJ arrangement and to what degree one can influence this process by choice of molecular connectivity. Compounds **13** and **20** have proven to function extremely well, but structural characterization reveals that the crystalline domains have very different aspect ratios and internal packing of chromophores. A composite picture of processing/morphology/function is therefore still missing and indicates that trial and error optimization will continue to be important for achieving major new advances. Perhaps more importantly, there is an appreciation of the need to shift to synthetic and device fabrication methods that are amenable to mass production.[40] It may very well be that the body of knowledge accumulated for spin-casted films does not directly translate because of the sensitivity toward deposition conditions. New materials must be developed that can yield high performance devices and take advantage of environmentally friendly syntheses and processes. Small molecules offer a favorable platform for which to address these challenges.

BIOGRAPHICAL INFORMATION

Jessica E. Coughlin received her B.S. in 2011 in chemistry and biochemistry from Florida State University. She is currently a doctoral candidate at the University of California, Santa Barbara pursuing novel molecular donor materials for organic photovoltaics.

Zachary B. Henson is a graduate student in the Department of Chemistry and Biochemistry at the University of California, Santa Barbara. He received his B.S. in chemistry from Indiana University—Bloomington and performed undergraduate research in the laboratory of Professor David E. Clemmer. His research interests include the design of narrow band gap conjugated polyelectrolytes and molecular semiconductors suitable for environmentally friendly processing.

Gregory C. Welch is an Assistant Professor of Chemistry and Canada Research Chair at Dalhousie University in Halifax, Nova Scotia. He obtained a B.Sc. in Chemistry from the University of Calgary in 2003 and worked in the laboratories of Tristram Chivers and Warren E. Piers. Gregory earned his Ph.D. at University of Windsor in 2008 under the supervision of Douglas W. Stephan. He then moved to UC-Santa Barbara, where he worked as a NSERC postdoctoral fellow. His research interests focus in the area of Printed Electronics, where he is developing new functional materials.

Guillermo C. Bazan is a Professor in the Departments of Materials and Chemistry & Biochemistry, and Director of the Center for Polymers and Organic Solids at the University of California, Santa Barbara. He received his B.Sc. from the University of Ottawa and his Ph.D. at MIT in 1991, working under the guidance of Professor Richard Schrock. His current interests concern the design of novel organic semiconducting materials for optoelectronic and bioelectronic applications, and the development of transition metal catalyzed synthesis of polymers.

FOOTNOTES

*To whom correspondence should be addressed.
The authors declare no competing financial interest.

REFERENCES

1 Dennler, G.; Scharber, M. C.; Brabec, C. J. Polymer-Fullerene Bulk-Heterojunction Solar Cells. *Adv. Mater.* **2009**, *21*, 1323–1338.
2 Brunetti, F. G.; Kumar, R.; Wudl, F. Organic electronics from perylene to organic photovoltaics: painting a brief history with a broad brush. *J. Mater. Chem.* **2010**, *20*, 2934.
3 Gendron, D.; Leclerc, M. New conjugated polymers for plastic solar cells. *Energy Environ. Sci.* **2011**, *4*, 1225.
4 Li, G.; Zhu, R.; Yang, Y. Polymer solar cells. *Nat. Photonics* **2012**, *6*, 153–161.
5 Roncali, J. Molecular Bulk Heterojunctions: An Emerging Approach to Organic Solar Cells. *Acc. Chem. Res.* **2009**, *42*, 1719–1730.
6 Sariciftci, N. S.; Smilowitz, L.; Heeger, A. J.; Wudl, F. Photoinduced electron transfer from a conducting polymer to buckminsterfullerene. *Science* **1992**, *258*, 1474–1476.
7 Bakulin, A. A.; Rao, A.; Pavelyev, V. G.; van Loosdrecht, P. H. M.; Pshenichnikov, M. S.; Niedzialek, D.; Cornil, J.; Beljonne, D.; Friend, R. H. The Role of Driving Energy and Delocalized States for Charge Separation in Organic Semiconductors. *Science* **2012**, *335*, 1340–1344.
8 Giridharagopal, R.; Ginger, D. S. Characterizing Morphology in Bulk Heterojunction Organic Photovoltaic Systems. *J. Phys. Chem. Lett.* **2010**, *1*, 1160–1169.
9 Günes, S.; Neugebauer, H.; Sariciftci, N. S. Conjugated Polymer-Based Organic Solar Cells. *Chem. Rev.* **2007**, *107*, 1324–1338.
10 Cheng, Y.-J.; Yang, S.-H.; Hsu, C.-S. Synthesis of Conjugated Polymers for Organic Solar Cell Applications. *Chem. Rev.* **2009**, *109*, 5868–5923.
11 Zhou, H.; Yang, L.; You, W. Rational Design of High Performance Conjugated Polymers for Organic Solar Cells. *Macromolecules* **2012**, *45*, 607–632.
12 Duan, C.; Huang, F.; Cao, Y. Recent development of push−pull conjugated polymers for bulk-heterojunction photovoltaics: rational design and fine tailoring of molecular structures. *J. Mater. Chem.* **2012**, *22*, 10416.

13 Mishra, A.; Bäuerle, P. Small Molecule Organic Semiconductors on the Move: Promises for Future Solar Energy Technology. *Angew. Chem., Int. Ed.* **2012**, *51*, 2020–2067.

14 Peet, J.; Kim, J. Y.; Coates, N. E.; Ma, W. L.; Moses, D.; Heeger, A. J.; Bazan, G. C. Efficiency enhancement in low-bandgap polymer solar cells by processing with alkane dithiols. *Nat. Mater.* **2007**, *6*, 497–500.

15 Coffin, R. C.; Peet, J.; Rogers, J.; Bazan, G. C. Streamlined microwave-assisted preparation of narrow-bandgap conjugated polymers for high-performance bulk heterojunction solar cells. *Nat. Chem.* **2009**, *1*, 657–661.

16 Tong, M.; Cho, S.; Rogers, J. T.; Schmidt, K.; Hsu, B. B. Y.; Moses, D.; Coffin, R. C.; Kramer, E. J.; Bazan, G. C.; Heeger, A. J. Higher Molecular Weight Leads to Improved Photoresponsivity, Charge Transport and Interfacial Ordering in a Narrow Bandgap Semiconducting Polymer. *Adv. Funct. Mater.* **2010**, *20*, 3959–3965.

17 Schilinsky, P.; Asawapirom, U.; Scherf, U.; Biele, M.; Brabec, C. J. Influence of the Molecular Weight of Poly(3-hexylthiophene) on the Performance of Bulk Heterojunction Solar Cells. *Chem. Mater.* **2005**, *17*, 2175–2180.

18 Welch, G. C.; Coffin, R.; Peet, J.; Bazan, G. C. Band gap control in conjugated oligomers via Lewis acids. *J. Am. Chem. Soc.* **2009**, *131*, 10802–10803.

19 Welch, G. C.; Bazan, G. C. Lewis acid adducts of narrow band gap conjugated polymers. *J. Am. Chem. Soc.* **2011**, *133*, 4632–4644.

20 Beaujuge, P. M.; Amb, C. M.; Reynolds, J. R. Spectral Engineering in π-Conjugated Polymers with Intramolecular Donor–Acceptor Interactions. *Acc. Chem. Res.* **2010**, *43*, 1396–1407.

21 Zalar, P.; Henson, Z. B.; Welch, G. C.; Bazan, G. C.; Nguyen, T.-Q. Color Tuning in Polymer Light-Emitting Diodes with Lewis Acids. *Angew. Chem., Int. Ed.* **2012**, *51*, 7495–7498.

22 Blouin, N.; Michaud, A.; Gendron, D.; Wakim, S.; Blair, E.; Neagu-Plesu, R.; Belletête, M.; Durocher, G.; Tao, Y.; Leclerc, M. Toward a Rational Design of Poly(2,7-Carbazole) Derivatives for Solar Cells. *J. Am. Chem. Soc.* **2008**, *130*, 732–742.

23 Zhou, H.; Yang, L.; Price, S. C.; Knight, K. J.; You, W. Enhanced Photovoltaic Performance of Low-Bandgap Polymers with Deep LUMO Levels. *Angew. Chem., Int. Ed.* **2010**, *49*, 7992–7995.

24 Steinberger, S.; Mishra, A.; Reinold, E.; Levichkov, J.; Uhrich, C.; Pfeiffer, M.; Bäuerle, P. Vacuum-processed small molecule solar cells based on terminal acceptor-substituted low-band gap oligothiophenes. *Chem. Commun.* **2011**, *47*, 1982.

25 Handy, S. T.; Wilson, T.; Muth, A. Disubstituted Pyridines: The Double-Coupling Approach. *J. Org. Chem.* **2007**, *72*, 8496–8500.

26 Welch, G. C.; Perez, L. A.; Hoven, C. V.; Zhang, Y.; Dang, X.-D.; Sharenko, A.; Toney, M. F.; Kramer, E. J.; Nguyen, T.-Q.; Bazan, G. C. A modular molecular framework for utility in small-molecule solution-processed organic photovoltaic devices. *J. Mater. Chem.* **2011**, *21*, 12700–12709.

27 Henson, Z. B.; Welch, G. C.; van der Poll, T.; Bazan, G. C. Pyridalthiadiazole-Based Narrow Band Gap Chromophores. *J. Am. Chem. Soc.* **2012**, *134*, 3766–3779.

28 Pivrikas, A.; Neugebauer, H.; Sariciftci, N. S. Influence of processing additives to nanomorphology and efficiency of bulk-heterojunction solar cells: A comparative review. *Sol. Energy* **2011**, *85*, 1226–1237.

29 Peet, J.; Senatore, M. L.; Heeger, A. J.; Bazan, G. C. The Role of Processing in the Fabrication and Optimization of Plastic Solar Cells. *Adv. Mater.* **2009**, *21*, 1521–1527.

30 Sun, Y.; Welch, G. C.; Leong, W. L.; Takacs, C. J.; Bazan, G. C.; Heeger, A. J. Solution-processed small-molecule solar cells with 6.7% efficiency. *Nat. Mater.* **2011**, *11*, 44–48.

31 Garcia, A.; Welch, G. C.; Ratcliff, E. L.; Ginley, D. S.; Bazan, G. C.; Olson, D. C. Improvement of Interfacial Contacts for New Small-Molecule Bulk-Heterojunction Organic Photovoltaics. *Adv. Mater.* **2012**, *24*, 5368–5373.

32 Liu, X.; Sun, Y.; Perez, L. A.; Wen, W.; Toney, M. F.; Heeger, A. J.; Bazan, G. C. Narrow-Band-Gap Conjugated Chromophores with Extended Molecular Lengths. *J. Am. Chem. Soc.* **2012**, *134*, 20609–20612.

33 van der Poll, T. S.; Love, J. A.; Nguyen, T.-Q.; Bazan, G. C. Non-Basic High-Performance Molecules for Solution-Processed Organic Solar Cells. *Adv. Mater.* **2012**, *24*, 3646–3649.

34 Leong, W. L.; Welch, G. C.; Kaake, L. G.; Takacs, C. J.; Sun, Y.; Bazan, G. C.; Heeger, A. J. Role of trace impurities in the photovoltaic performance of solution processed small-molecule bulk heterojunction solar cells. *Chem. Sci.* **2012**, *3*, 2103–2109.

35 Takacs, C. J.; Sun, Y.; Welch, G. C.; Perez, L. A.; Liu, X.; Wen, W.; Bazan, G. C.; Heeger, A. J. Solar cell efficiency, self-assembly, and dipole-dipole interactions of isomorphic narrow-band-gap molecules. *J. Am. Chem. Soc.* **2012**, *134*, 16597–16606.

36 Welch, G. C.; Bakus, R. C., II; Teat, S. J.; Bazan, G. C. Impact of Regiochemistry and Isoelectronic Bridgehead Substitution on the Molecular Shape and Bulk Organization of Narrow Bandgap Chromophores. *J. Am. Chem. Soc.* **2013**, *135*, 2298–2305.

37 Yasuda, T.; Sakai, Y.; Aramaki, S.; Yamamoto, T. New Coplanar (ABA) n-Type Donor–Acceptor π-Conjugated Copolymers Constituted of Alkylthiophene (Unit A) and Pyridazine (Unit B): Synthesis Using Hexamethylditin, Self-Organized Solid Structure, and Optical and Electrochemical Properties of the Copolymers. *Chem. Mater.* **2005**, *17*, 6060–6068.

38 Peng, Q.; Liu, X.; Su, D.; Fu, G.; Xu, J.; Dai, L. Novel Benzo[1,2-b:4,5-b′]dithiophene-Benzothiadiazole Derivatives with Variable Side Chains for High-Performance Solar Cells. *Adv. Mater.* **2011**, *23*, 4554–4558.

39 Zhang, Y.; Chien, S.-C.; Chen, K.-S.; Yip, H.-L.; Sun, Y.; Davies, J. A.; Chen, F.-C.; Jen, A. K. Y. Increased open circuit voltage in fluorinated benzothiadiazole-based alternating conjugated polymers. *Chem. Commun.* **2011**, *47*, 11026–11028.

40 Søndergaard, R.; Hösel, M.; Angmo, D.; Larsen-Olsen, T. T.; Krebs, F. C. Roll-to-roll fabrication of polymer solar cells. *Mater. Today* **2012**, *15*, 36–49.